Supplemental Material for "Biogenic and Biomass Burning Aerosol in a Boreal Forest at Hyytiala, Finland during HUMPPA-COPEC 2010"

S.1 Organic Acids Comparison

Correlation between the sum of all functional groups, measured by FTIR, and the sum of all particle phase organic acids between *m/z* 100 to 500 (averaged during filter sampling interval), measured by APCI-MS, is shown in Figure S1. Linear regression results in r = 0.90, showing a good agreement between those techniques. The highest AMS O/C ratio of 0.81 was measured on 24 July (FIN 133, filter number), the day with the sole nucleation event of the campaign. Due to low organic aerosol masses, both instruments measured values close to zero, however, the high O/C ratio might indicate that organic acids play a key role during nucleation. On the days 29 July (FIN155), 8 August and 9 August (FIN184, FIN186), when biomass burning aerosol arrived at Hyytiälä, both instruments show highest signals in mass and FTIR indicates O/C ratios which are above the campaign average. The correlations between the FTIR and APCI-MS signals were all quite high, with carboxylic acid functional groups having r = 0.84, and other corresponding groups even higher: alcohol (0.86), alkane (0.85), amine (0.88), and carbonyl (0.93) groups.

S.2 Factor Analysis

Positive Matrix Factorization (PMF) was applied to FTIR and AMS spectra to identify robust, linearly independent components representing local and regional sources of OM. Factor solutions were analyzed by number of factors, rotational values (FPEAK), and starting seed values. In depth factor selection criteria are described below for FTIR and AMS factors.

S.2. 1 FTIR Factor Analysis

PMF was applied to 65 submicron FTIR spectra. The portion of the spectra with quantifiable peaks (3800-1500 cm^{-1}, with the exclusion of the Teflon interference) was used for the analysis and the standard deviation of each wavenumber for the back filters was used as the uncertainty for PMF [*Russell et al*., 2009]. Robust mode was used and rotational values (FPEAKs) of ±1.2, ±1.0, ±0.8, ±0.6, ±0.4, ±0.2 and 0 were evaluated. All rotations were examined and it was observed that FPEAKs >0.2 resulted in unrealistic spectra (i.e. single functional group or lacking alkane functional group), consistent with *factor splitting* [*Ulbrich et al*., 2009]. Minimum

$Q/Q_{expected}$, as described by Paatero et al. [2002], was used for FPEAK selection (Figure S2), and solutions of FPEAK of 0 were selected. Seed values of 0, 10, and 100 were investigated to check for robustness of the solutions. Amongst the seed values, correlations (r) of the factor spectra and time series were >0.95, showing consistency amongst the solutions. A seed value of 0 was chosen to represent the FTIR solution.

A set of solutions, ranging from 2- to 7-factors were examined. $Q/Q_{expected}$ decreased with increasing number of factors in the solution (Figure S3), suggesting a higher number of factors better fit the observed FTIR spectra. However, solutions with > 4 factors resulted in unrealistic spectra, which contained no real physical meaning. Additionally, solutions with > 4 factors generated unidentified factors, small factors (< 5% OM), or factors that correlated strongly (r > 0.65) with respect to time or spectral signature with other factors in the set of solutions, while 2- and 3-factor solutions underrepresented total OM (< 85% OM). The 4-factor solution recreated 95% of the total OM and generated linearly-independent factors with specific source signatures.

S.2.2 AMS Factor Analysis

Unit-mass resolution PMF was performed on C-ToF-AMS data. Data and error matrices were generated using SQUIRREL (version 1.51) with Igor Pro 6.12 (WaveMetrics, Lake Oswego, OR). The PET software and analysis described by Ulbrich et al. [2009] were used to perform PMF. Due to low signal to noise (S/N), ion fragments with m/z > 100 were removed from the analysis. Ion fragments with 0.2 < S/N < 2 were downweighted by a factor of 2, in addition the CO_2^+- ions and their fragments (m/z 16, 17, 18, 28, and 44) were downweighted by a factor of 10 due to the highly oxygenated nature of aerosol at Hyytiälä [*Paatero and Hopke*, 2003; *Ulbrich et al*., 2009]. Additionally, m/z 24 was downweighted by a factor of 10 because of a high sum of squared residuals observed for this fragment. Robust mode was used and FPEAKs of ±1.2, ±1.0, ±0.8, ±0.6, ±0.4, ±0.2 and 0 were evaluated. $Q/Q_{expected}$ was found to decrease with FPEAK (Figure S2); however, minimum $Q/Q_{expected}$ (FPEAK=0) was not selected for the final solution. Mathematically ideal solutions (FPEAK=0) are not necessarily the best solution, if the spectra are unrealistic or have undergone *factor splitting* [*Ulbrich et al*., 2009]. Solutions for FPEAK > -0.4 contained one or more factors that lacked m/z 43 ($C_2H_3O^+$ and $C_3H_7^+$), a predominant fragment, suggesting the solutions from these rotational values were unrealistic and over split.

FPEAK of -0.4 was selected to best represent the solution.

Solutions with 2- to 7-factors were analyzed to determine the set of factors that best describe the measured organic fragments at Hyytiälä. Solutions with > 4 factors resulted in factors that were small (< 7% OM) and were highly correlated in time ($r > 0.8$), indicating some factors had split. Additionally solutions with 4 or more factors contained factors that lacked m/z 43 or 44 or had other unrealistic spectra, also suggesting factor splitting. The 2-factor solution was able to reconstruct 97% of the OM variability, but this was improved by allowing 3 factors, which reconstructed 100%. The 3-factor solution was found to have factors with substantial masses (> 25% OM) and had strong correlations to organic tracers, in addition to weak temporal correlations among the factors. For such reasons, the 3-factor solution was chosen to represent OM components measured at Hyytiälä.

S.3 Biogenic and Biomass Burning Separation in FTIR Factors

The three-factor solution contained $FFC1_{FTIR}$, BIO_{FTIR}, and BB_{FTIR}, but only explained 85% of OM variability. However, BIO_{FTIR}, and BB_{FTIR} were similar both temporally and chemically between the three and four factor split (Figure S6). $FFC2_{FTIR}$ presented only in the four-factor solution, with the majority of the mass arising from $FFC1_{FTIR}$ and a small fraction evolving from the BIO_{FTIR} mass in the three-factor solution. Such robustness in the biogenic and biomass burning factor spectra and profile strength suggests that biogenic and biomass burning aerosol separated completely, and the factor OM of each source is chemically consistent.

S.4 Single Particle Types from Biomass Burning Emissions

Single particles were impacted on silicon nitride windows (Si_3N_4, Silson Ltd.) on 26 and 29 July and frozen at 0°C prior to analysis. Single particles were analyzed at the Advanced Light Source (Lawrence Berkeley National Laboratory, Berkeley, CA) on Beamline 5.3.2 by Scanning Transmission X-ray Microscopy with Near-Edge X-ray Absorption Fine Structure (STXM-NEXAFS) spectroscopy. Single particles were analyzed at the carbon K-edge for single-particle organic functional groups by scanning through energy levels 278-320 eV [*Kilcoyne et al.*, 2003]. Spectra were processed using an automated algorithm to provide information on single-particle organic functional group abundance, size, and morphology [*Takahama et al.*, 2007; *Takahama et*

al., 2010].

46 particles from three days (26, 27, and 29 July) were sampled and analyzed by STXM-NEXAFS. All 46 particles were collected on days that had substantial OM contributions from biomass burning emissions that originated in western Russia. The majority of the sampled particles were 1-3 μm in diameter. The NEXAFS spectra had clear absorption by carboxylic acid groups, which suggests the particles had substantial secondary organic mass components. The single-particle spectra were categorized by hierarchical Ward analysis [*Ward*, 1963] and compared to 14 types of single particles identified by Takahama et al. [2007] (Figure 6).

Cluster 1 particles (n=21) showed strong alkene/aromatic group (285.0 eV), carboxylic acid group (288.7 eV), and potassium (297.4 and 299.9 eV) absorption (Figure 6a). Particles in Cluster 1 differed from the particle types identified by Takahama et al. [2007], as Type F particles were the only particles to contain strong K absorption. However, Type F particles also contained CO_3^{2-} (290.4 eV), a signature for dust particles that was not identified in Cluster 1 particles. Potassium is a typical tracer of primary pyrogenic emissions [*Andreae*, 1983], likely from volatilization and reactions within the vegetation during burning that results in the nucleation and condensation of potassium-salt particles [*Gaudichet et al*., 1995]. Tarballs, spherical HULIS-like particles, have often been identified in biomass burning emissions [*Posfai et al*., 2003; *Tivanski et al*., 2007]; however, no tarball-like particles were identified in the 46 particles sampled during biomass burning periods. Potassium-rich single particles have been identified in aged smoke plumes, including potassium-salt with amorphous organic coatings and organic particles with small potassium-salt inclusions [*Li et al*., 2003]. These organic potassium-salt particles are believed to contain water-soluble organic compounds found in biomass smoke, making them important cloud condensation nuclei [*Posfai et al*., 2003], although other sources have also been identified [*Pohlker et al*., 2012].

The remaining clusters 2 and 3 resembled particle types identified by Takahama et al. [2007] (Figure S8). Cluster 2 particles showed strong carboxylic acid group absorption at 288.7 eV and were the second-most dominant particle type (n=20). Particles in Cluster 2 were spherical and spectra were similar to Type A particles, which are likely the result of atmospheric processing

[Takahama et al. 2007] (Figure S8b). Cluster 3 particles (n=5) were characterized by strong alkene or aromatic group absorption at 285.0 eV and resembled Type H particles from Takahama et al. [2007], which likely have combustion origins (Figure S8c) since the magnitude of the 285.0 eV peak is characteristic of high fractions of elemental or other pi bonded carbon.

Supplemental Figures

Figure S1 - (a) FTIR OM compared with filter-averaged AMS OM (solid fit line: y = 0.9x + 0.15, r = 0.94). Dashed line represents 1:1. (b) Correlation between FTIR OM and the filter-averaged sum of all particle-phase signals between *m/z* 100 to 500 measured by APCI-MS (solid fit line: y = 8.96e+04x – 1.2e+05, R = 0.90). Arbitrary units (a.u.) were used for APCI-MS organic acids.

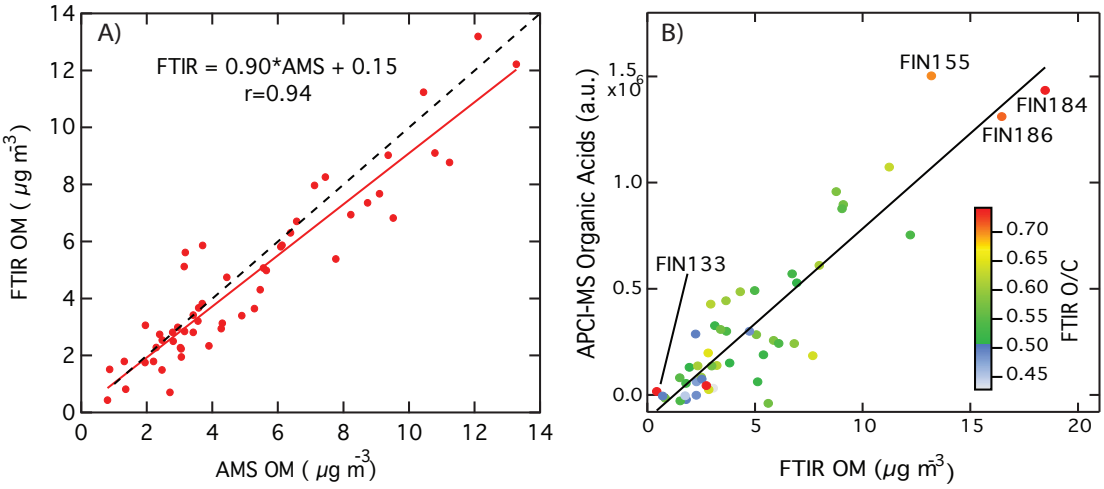

Figure S2 –Dependence of $Q/Q_{expected}$ on FPEAK rotation for FTIR (red, left axis) and AMS (blue, right axis) factors. Solid squares indicate selected solution for FTIR and AMS factors.

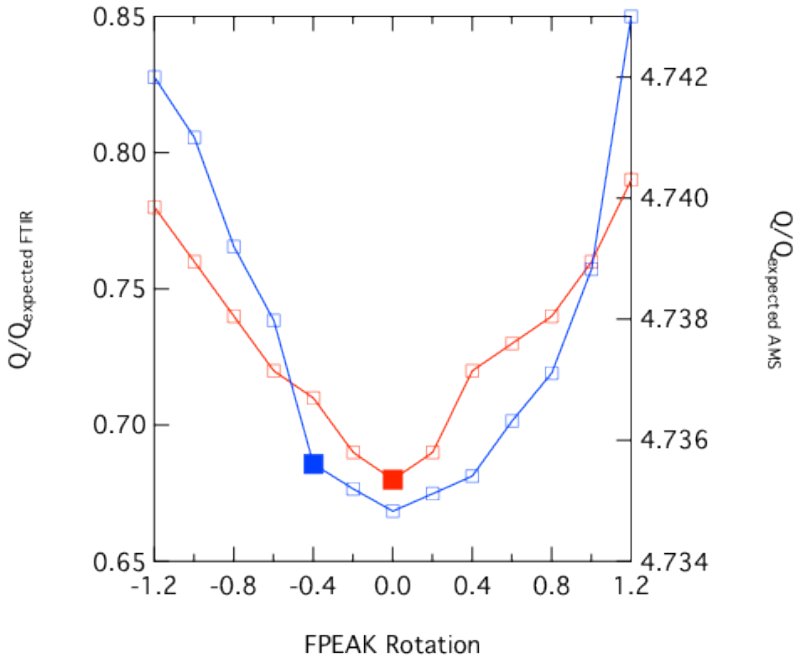

Figure S3 – Dependence of $Q/Q_{expected}$ on number of factors in a set of solutions for FTIR (red, left axis) and AMS (blue, right axis). Solid circles indicate selected solution for FTIR and AMS factors.

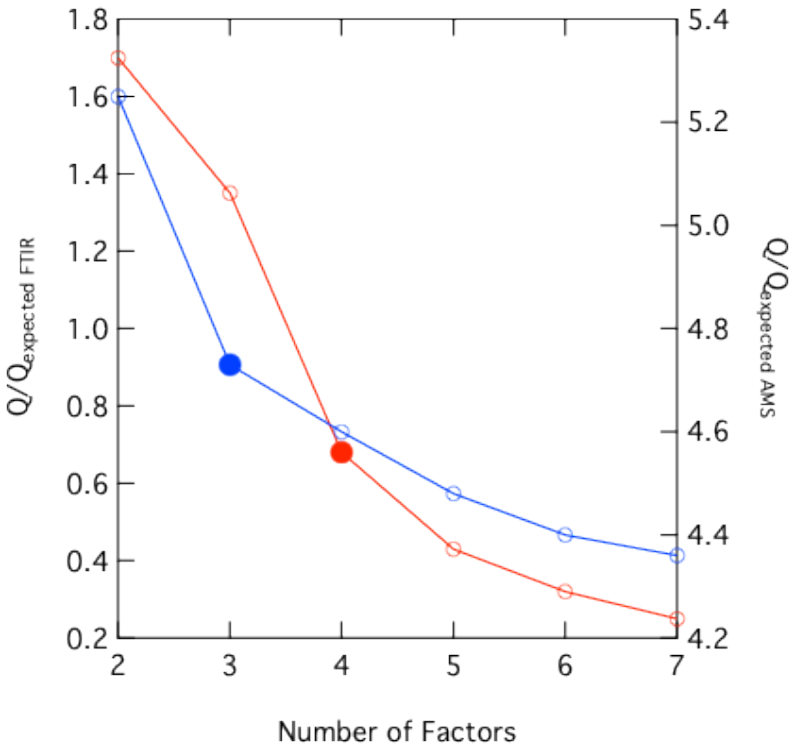

Figure S4 - Correlations coefficients (r) of FTIR factors and source markers. Colors indicate strength of correlation coefficient, strong ($r > 0.75$, red), moderate ($0.5 < r < 0.75$, green), weak ($0.25 < r < 0.5$, light blue), no correlation ($-0.25 < r < 0.25$, purple).

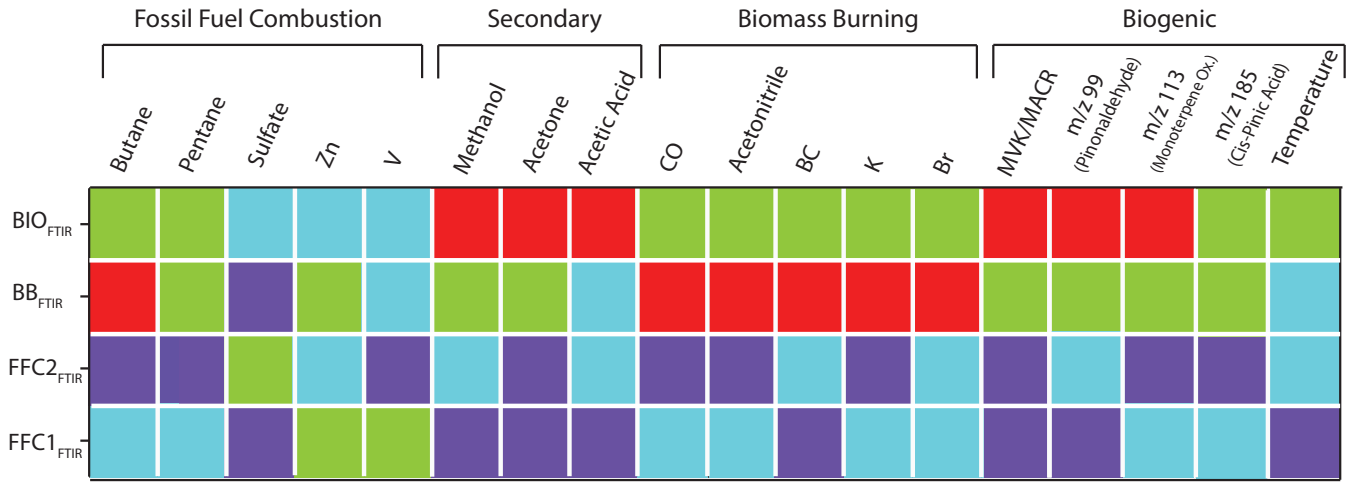

Figure S5 - Correlations coefficients (r) of AMS factors and source markers. Colors indicate strength of correlation coefficient, strong ($r > 0.75$, red), moderate ($0.5 < r < 0.75$, green), weak ($0.25 < r < 0.5$, light blue), no correlation ($-0.25 < r < 0.25$, purple).

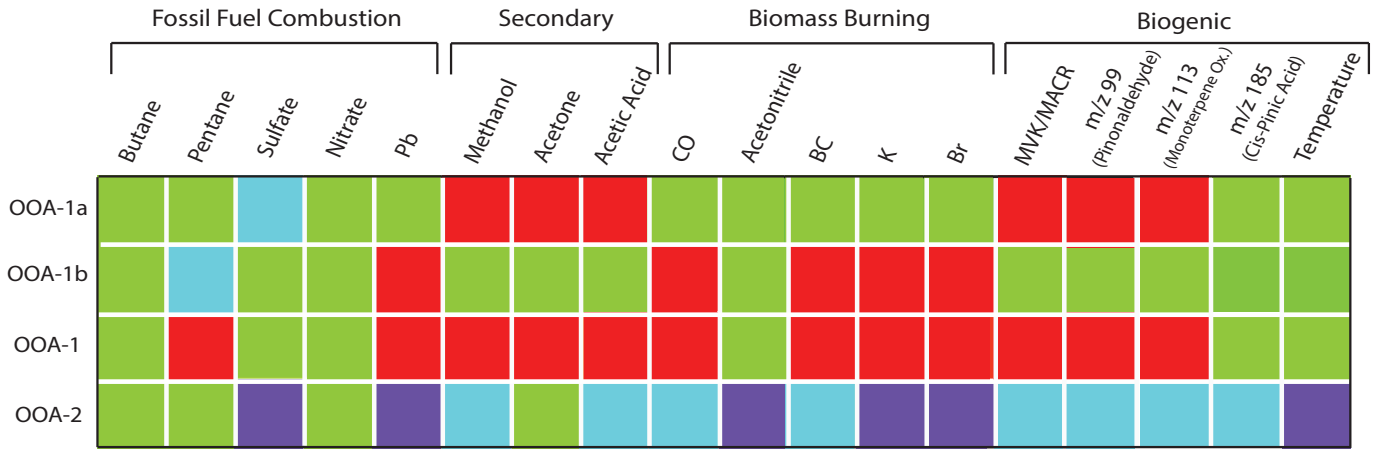

Figure S6 – Time series of submicron OM reconstructed from PMF analysis on FTIR spectra of the (top) four-factor solution with Combustion 1 (black), Combustion 2 (brown), Biomass Burning (red), and Biogenics (green) and (bottom) three-factor solution. Arrows indicate split of Combustion 1 factor between the three-factor and four-factor solution. Color bars on top of figure indicate periods of stressed boreal conditions (green) and biomass burning (red).

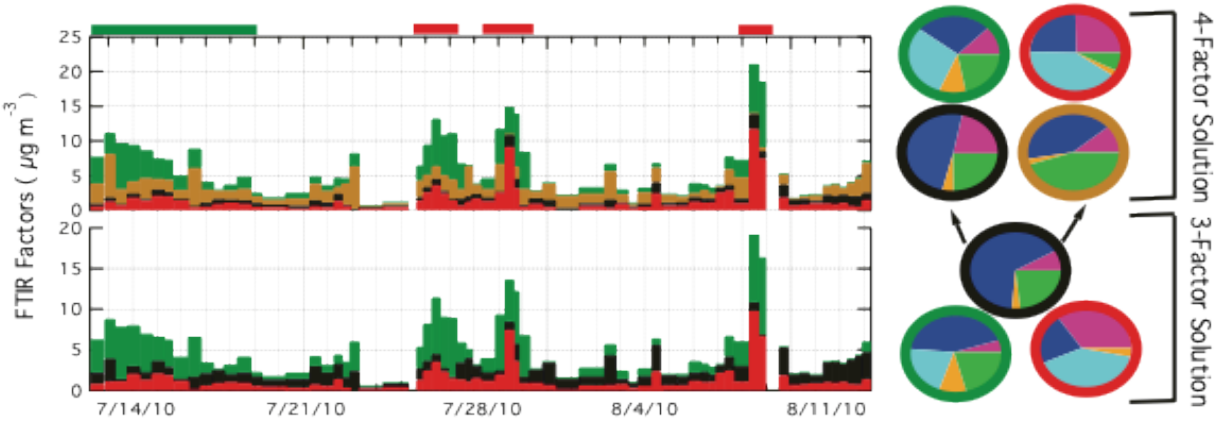

Figure S7 – C-ToF- AMS organic aerosol composition in the [*Ng et al*., 2010] triangle space (f_{44} vs f_{43}). Hyytiälä organic aerosol (grey points) fall mostly within Ng triangle space, with bulk organic aerosol (campaign average: grey triangle) also falling inside triangle space. Factors from 3-factor PMF solution are plotted, OOA-1a (green), OOA-1b (red), and OOA-2 (black).

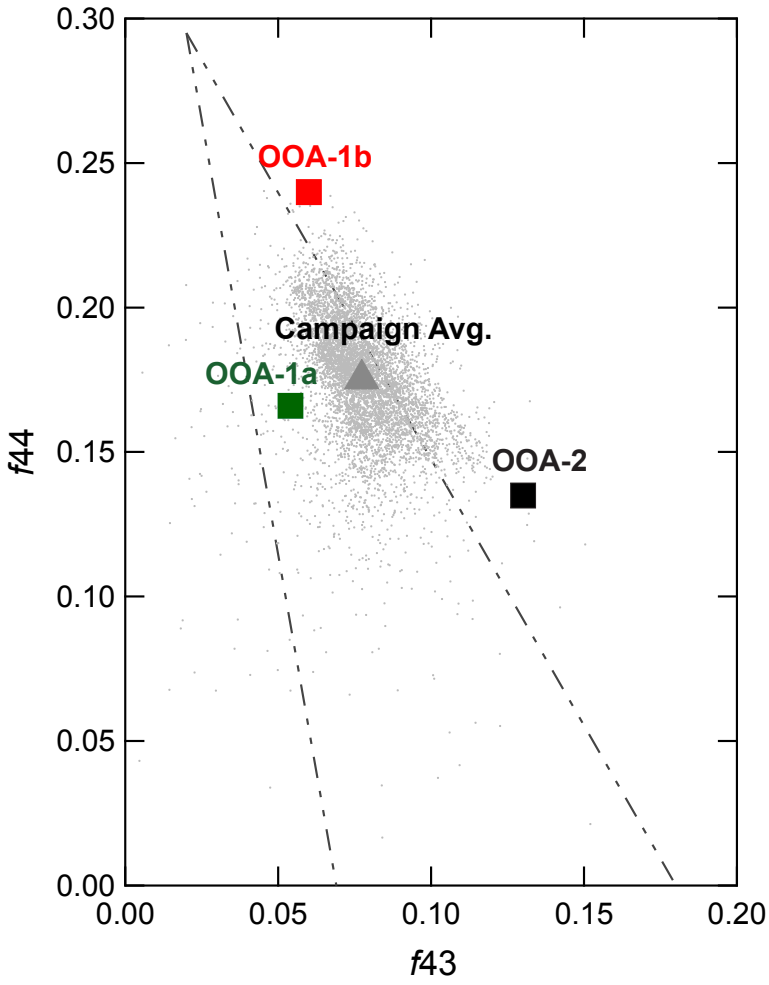

Figure S8 – Normalized single-particle spectra clustered into three categories: (A) Cluster I, (B) Cluster II, and (C) Cluster III. Black line indicates cluster average and grey lines represent individual particle spectra. Red lines represent type "a" and "h" [identified in [*Takahama et al.*, 2007]] particles for Cluster II and III respectively. Yellow vertical lines indicate absorptions of specific organic and inorganic functional groups: 285.0 eV alkene/aromatics, 286.7 eV ketonic carbonyl, 287.7 eV carboxylic carbonyl, 289.5 eV alcohol, 290.4 eV carbonate, and 297.4 and 299.9 eV for potassium. (D) Distribution of 46 organic-containing single particles binned by spherical equivalent geometric diameter. Images inset in (A)-(C) show absorbance images at 288.85 eV and represent typical single-particle geometries of each cluster.

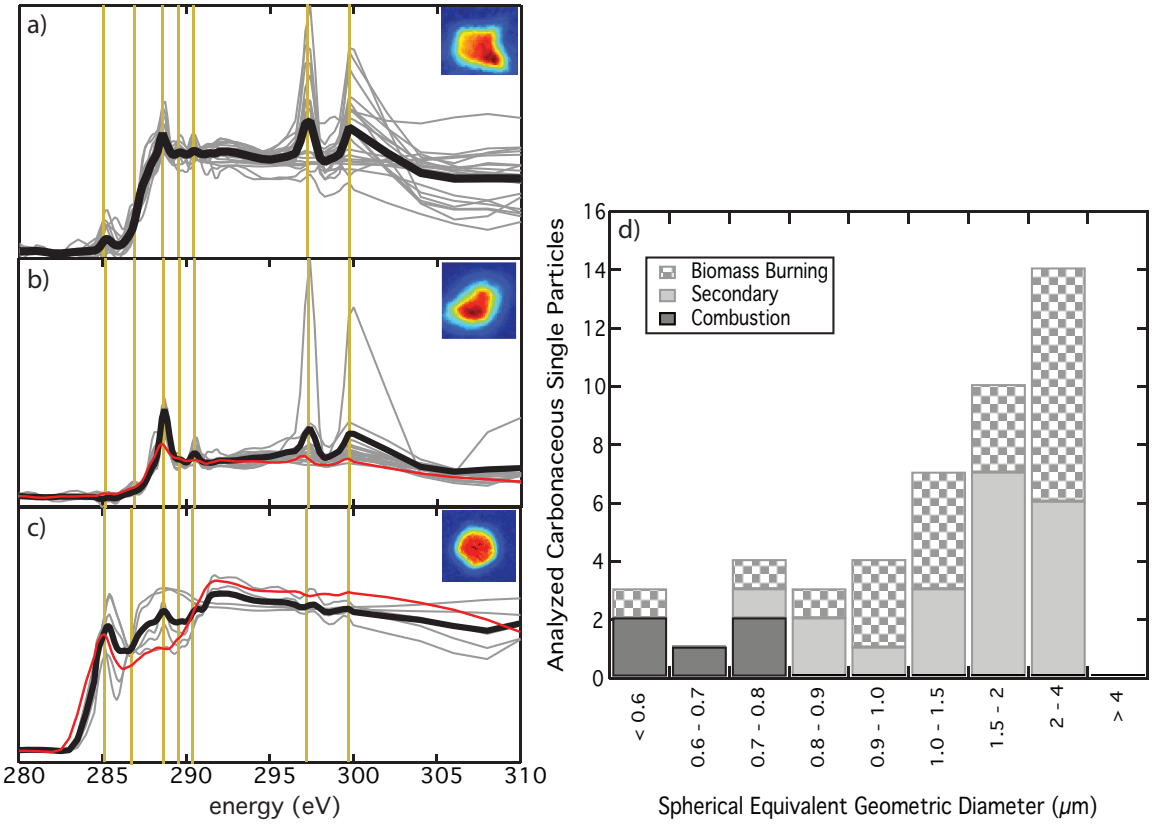

References

Andreae, M. O. (1983), Soot carbon and excess fine potassium - long-range transport of combustion-derived aerosols, Science, 220(4602), 1148-1151.

Gaudichet, A., et al. (1995), Trace-elements in tropical african savanna biomass burning aerosols, Journal of Atmospheric Chemistry, 22(1-2), 19-39.

Kilcoyne, A. L. D., et al. (2003), Interferometer-controlled scanning transmission x-ray microscopes at the advanced light source, Journal of Synchrotron Radiation, 10, 125.

Li, J., et al. (2003), Individual aerosol particles from biomass burning in southern africa: 2, compositions and aging of inorganic particles, Journal of Geophysical Research-Atmospheres, 108(D13), 12.

Ng, N. L., et al. (2010), Organic aerosol components observed in northern hemispheric datasets from aerosol mass spectrometry, Atmospheric Chemistry and Physics, 10(10), 4625-4641.

Paatero, P., et al. (2002), Understanding and controlling rotations in factor analytic models, Chemometrics and Intelligent Laboratory Systems, 60(1-2), 253-264.

Paatero, P., and P. K. Hopke (2003), Discarding or downweighting high-noise variables in factor analytic models, Analytica Chimica Acta, 490(1-2), 277-289.

Pohlker, C., et al. (2012), Biogenic potassium salt particles as seeds for secondary organic aerosol in the amazon, Science, 337(6098), 1075-1078.

Posfai, M., et al. (2003), Individual aerosol particles from biomass burning in southern africa: 1. Compositions and size distributions of carbonaceous particles, Journal of Geophysical Research-Atmospheres, 108(D13).

Russell, L. M., et al. (2009), Oxygenated fraction and mass of organic aerosol from direct emission and atmospheric processing measured on the r/v ronald brown during texaqs/gomaccs 2006, Journal of Geophysical Research-Atmospheres, 114.

Takahama, S., et al. (2007), Classification of multiple types of organic carbon composition in atmospheric particles by scanning transmission x-ray microscopy analysis, Atmospheric Environment, 41(40), 9435-9451.

Takahama, S., et al. (2010), Coatings and clusters of carboxylic acids in carbon-containing atmospheric particles from spectromicroscopy and their implications for cloud-nucleating and optical properties, Journal of Geophysical Research-Atmospheres, 115(D01202).

Ulbrich, I. M., et al. (2009), Interpretation of organic components from positive matrix factorization of aerosol mass spectrometric data, Atmospheric Chemistry and Physics, 9(9), 2891-2918.

Ward, J. H. (1963), Hierarchical grouping to optimize an objective function, Journal of the American Statistical Association, 58.